ISSN 1330-3651 (Print), ISSN 1848-6339 (Online)
Received: 29 April 2025; Accepted: 28 July 2025

https://doi.org/10.17559/TV-20250429002632
Original scientific paper

Design and Validation of a Rotational End-Effector with a Stalk-Bending and Separation Mechanism for Apple Harvesting

Jianguo ZHOU, Shiwei WEN, Deyi ZHANG, Jun CHEN*, Yu CHEN, Guangrui HU

Abstract: Traditional gripping end-effectors often damage fruit due to structural complexity and uneven force distribution. To overcome these limitations, this study proposes a rotational end-effector that safely separates the stalk from the branch through a bending action. First, the design scheme and operating principle were established based on harvesting requirements. A rotational harvesting strategy was then formulated using statistical data, notably an average stalk length of 21.98 ± 4.33 mm. Subsequently, a composite mechanical model was developed, which enabled the derivation of critical conditions for stalk separation through theoretical analysis. Next, finite element simulations were conducted to assess the bending effects and stress distribution, confirming the end-effector's capability to protect the apple's surface. Finally, the end-effector was integrated into a harvesting robot and underwent extensive field experiments. Key parameters such as motor torque, motor speed, and opening width were optimized using response surface methodology (RSM). Under conditions of a 31.43 rpm motor speed, 6.22 N·m motor torque, and a 34.16 mm opening width, the theoretical harvesting success rate reached 90.17%, while the actual success rate was 89%, demonstrating a negligible discrepancy. These results indicate that the rotational end-effector effectively preserves apple quality and holds promising prospects for practical application.

Keywords: apple harvesting; field packing experiments; finite element analysis; parameter optimization; rotational end-effector; stalk bending

1 INTRODUCTION

Apples are among the most widely cultivated economic crops worldwide and exhibit distinct seasonal harvesting characteristics [1, 2]. Traditional manual harvesting methods are labor-intensive and incur high costs [3]. With rising labor expenses and increasing efficiency demands, mechanized harvesting has become a key trend in modern orchard production [4]. In recent years, rapid advances in automation have accelerated the development of harvesting robots [5]. As a critical component, the end-effector directly influences both harvesting efficiency and fruit quality [6, 7]. However, existing end-effectors for apple harvesting robots still face challenges such as fruit damage, structural complexity, and limited operational convenience [8, 9]. Addressing these issues is the primary motivation behind the design of the novel end-effector presented in this study.

Currently, harvesting robots employ several types of end-effectors, including gripper, vacuum, cutting, and composite types [10, 11]. Each type has distinct advantages and is designed for specific harvesting scenarios. For instance, gripper end-effectors rely on mechanical force to secure fruits [12]. Li et al. [13] designed a three-finger gripper end-effector for pear harvesting. This device integrates force and posture control within soft fingers to accommodate different fruit sizes and shapes. However, excessive gripping force may damage the fruit surface and reduce market value. Vacuum end-effectors use suction to achieve rapid harvesting [14]. Lu et al. [15] developed a vacuum apple harvesting end-effector with flexible suction cups. This design enhanced adhesion and achieved a success rate of up to 89% in field experiments. Nevertheless, variations in fruit size and rough or wet surfaces can impair suction performance. Cutting end-effectors, which harvest fruits by cutting the stalk, are suitable for fruits that are difficult to grip [16]. Zhao et al. [17] proposed a cutting end-effector for broccoli harvesting. They developed a kinetic model and achieved an overall harvesting success rate of 93.3% in experiments. However, the complex mechanical structure and control system may result in higher failure rates and maintenance costs.

Composite end-effectors integrate multiple harvesting mechanisms [18]. For example, Hohimer et al. [19] improved a vacuum-gripper for apple harvesting by incorporating flexible fingers to enhance adaptability. However, experiments showed that while increasing working air pressure improved response speed, the overall success rate remained at only 67%. In another study, Park et al. [20] developed a gripper-cutting end-effector for cucumber harvesting and investigated the optimal harvesting sequence. However, the complex working environment and insufficient gripping accuracy led to an average harvesting success rate of only 56.6%. Similarly, Gao et al. [21] designed a vacuum-gripper end-effector for tomato harvesting that employed a combined pulling and bending mode. Nevertheless, the harvesting success rate was only 66.3%, primarily due to insufficient suction force.

In summary, the aforementioned end-effectors perform well under specific conditions. However, most rely on direct gripping or simple pulling, which can cause fruit surface damage. Moreover, these systems generally exhibit inadequate adaptability and low efficiency in practical applications. To address these limitations, this study proposes an apple harvesting end-effector utilizing a stalk bending and separation mechanism. The design applies a controlled bending force to the stalk, which achieves efficient and gentle separation from the branch. At the same time, it minimizes fruit damage and maintains high harvesting efficiency.

This study aims to evaluate the actual working performance of the newly designed end-effector and to propose a novel method for apple harvesting. The paper systematically describes the design and experimental process. First, an overall design scheme is developed, detailing the structural components and operating principles. Next, a theoretical analysis is conducted to derive the critical force required for stalk separation. Finite element analysis is then performed to simulate the operational process and obtain key mechanical data, such as stress distribution on the stalk and apple surface. Finally,

extensive field experiments are conducted to evaluate the harvesting performance under various operating conditions. Response surface methodology is then applied to optimize the key parameters.

2 MATERIALS AND METHODS

2.1 Agronomic Conditions and Design Principles

The cultivation practices and growth characteristics of apple orchards significantly affect the operational workspace and overall adaptability of the end-effector [22, 23]. Therefore, a thorough understanding of the target orchard's agronomic conditions is essential for designing the end-effector. Shaanxi Province (34°21'N, 107°14'E) is one of the major apple-producing regions in China. In this study, the primary production area of Fuji apples in central Shaanxi Province was selected as the experiment site (Fig. 1a). The site adopts a cultivation mode involving dwarfing rootstock and high-density planting to form a compact fruit tree structure suitable for mechanized harvesting. Field measurements indicate that the average tree height is 4.5 m, with a row spacing of 3.5 m and an inter-tree spacing of 1.2 m. Furthermore, apples predominantly grow at heights between 1.1 m and 2.5 m above the ground, providing ample operational space for the end-effector.

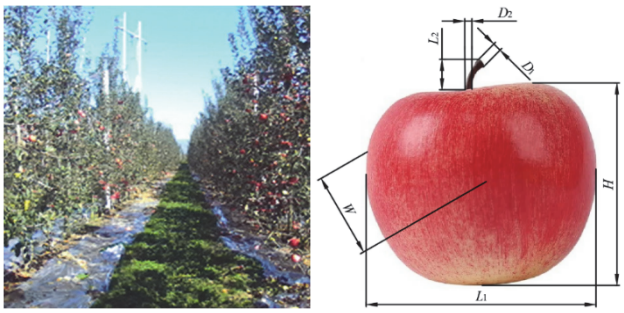

(a) Orchard environment (b) Measuring main dimensions

Figure 1 Agronomic conditions and main fruit dimensions

Due to natural variability in apple size and shape during growth [24], the primary dimensions of the apple, stalk, and branch were systematically measured. One hundred apples were randomly selected, and their three-dimensional (3D) measurements (Fig. 1b) were recorded using a digital vernier caliper. The Shapiro-Wilk test [25] confirmed that the data followed a normal distribution ($p > 0.05$, Tab. 1), thereby providing robust statistical support for the structural design of the end-effector.

Table 1 S-W test results of dimensions

Dimension	Meaning	Average value / mm	Standard deviation / mm	*P* value of S-W test
L_1	Apple length	80.93	5.71	0.478
W	Apple width	78.26	5.77	0.343
H	Apple height	71.33	5.28	0.492
L_2	Stalk length	21.98	4.33	0.671
D_1	Stalk large end diameter	3.36	0.51	0.546
D_2	Stalk small end diameter	2.18	0.37	0.215
D_3	Branch diameter	12.31	2.05	0.228

Harvesting damage directly affects the quality and market value of apples [26]. Consequently, adopting strategies to minimize fruit damage is essential for the end-effector's design. Observations of manual harvesting indicate that workers typically secure the apple using two fingers while gently pushing the stalk with a third finger (Fig. 2). In this process, a modest tangential force is applied. This force takes advantage of the lower tangential bonding force at the stalk-branch junction compared to the normal force, thereby facilitating the separation of the stalk from the branch. This approach is further supported by relevant literature [27, 28].

Figure 2 Schematic diagram of manual harvesting

Based on these observations and literature, this study proposes three design principles for the end-effector:

(1) The harvesting action should be simple and efficient to complete the task quickly, thereby enhancing operational efficiency.

(2) The end-effector should minimize direct contact with the apple surface to reduce fruit damage and preserve appearance.

(3) The stalk should remain intact during harvesting to prevent deterioration or decay resulting from detachment and to minimize moisture loss.

2.2 Design Scheme and Working Principle

Based on the previous analysis, this study proposes a rotational end-effector for apple harvesting (Fig. 3). The device consists of a harvesting barrel, a transmission block, a motor, a mounting block, a driver, a battery, and a baffle. The top of the harvesting barrel features an opening designed for positioning the stalk. In addition, multiple holes are integrated into the barrel to reduce weight while maintaining structural strength. The motor drives the harvesting barrel to rotate through the transmission block, thereby applying a controlled bending force to the stalk. This bending action gently separates the stalk from the branch. The driver precisely controls the motor's speed and direction, ensuring that the harvesting process is both efficient and accurate. The baffle prevents apples from falling due to vibrations, thus ensuring harvesting safety. Finally, the end-effector is securely attached to the robotic arm via a mounting block.

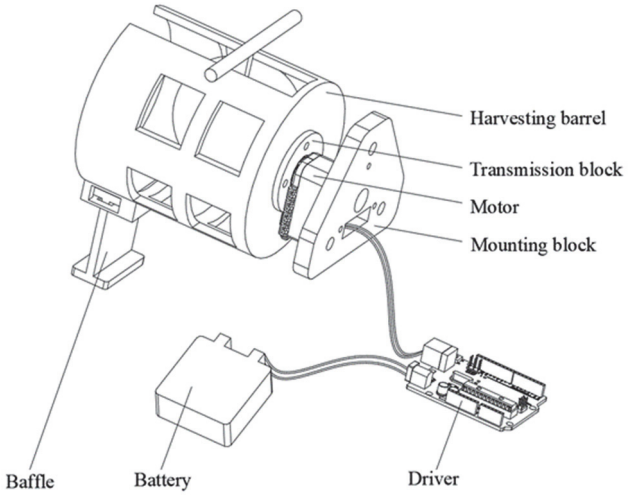

Figure 3 Schematic diagram of the rotational end-effector

During operation, the end-effector is accurately guided to the target area through coordinated control by the operating system and the robotic arm. A detailed description of the implementation process is provided in the harvesting robot solution module. Next, the driver activates the motor, causing the harvesting barrel to rotate to a preset angle. This rotation bends and separates the stalk from the branch. Simultaneously, the baffle automatically descends under gravity to prevent the harvested apples from falling. Finally, the robotic arm transports the apple to the designated placement area. The driver then commands the motor to rotate again, allowing the baffle to release the apple into the collection box. This cycle is repeated continuously to ensure efficient and uninterrupted apple harvesting.

2.3 Force Analysis of the Harvesting System

To analyze the specific loading conditions applied by the end-effector on the stalk, a composite force model comprising the branch, stalk, apple, and end-effector was developed (Fig. 4a). For simplicity, the stalk is approximated as a vertical cantilever beam. The upper end is connected to the branch, which generally remains stationary during harvesting; hence, the connection is considered fixed. The lower end is connected to the apple. Because the apple's mass is negligible relative to the load applied by the end-effector, it is omitted in the analysis. As apples mature, the binding force between the stalk and the branch gradually decreases, which is beneficial for the picking process.

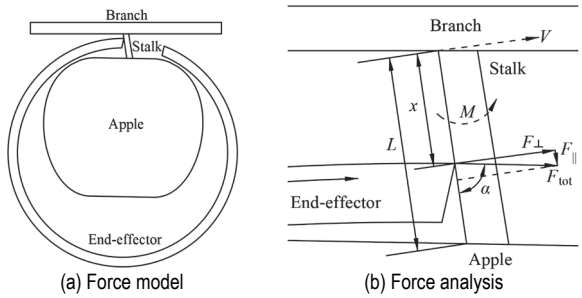

(a) Force model (b) Force analysis

Figure 4 Force analysis of the harvesting system

As the rotation angle changes, the load direction on the stalk also varies (Fig. 4b). Defining the angle between the total load F_{tot} and the stalk axis as α, the load can be decomposed into a perpendicular component $F_{\perp}$, which induces radial bending, and a parallel component $F_{\parallel}$, which causes axial tension or compression (Eq. (1) and (2)).

$$F_{\perp} = F_{tot} \sin\alpha \tag{1}$$

$$F_{\parallel} = F_{tot} \cos\alpha \tag{2}$$

It is generally considered that stalk fracture is primarily attributed to the bending moment M and shear force V generated by $F_{\perp}$ (Eq. (3) and (4)).

$$M = F_{\perp} x \tag{3}$$

$$V = F_{\perp} \tag{4}$$

where x is the distance between the contact point of the end-effector with the stalk and the branch-stalk connection (m).

In addition, the maximum bending stress σ_{max} at the connection between the circular-section stalk and the branch is calculated using Eq. (5), the maximum shear stress τ_{max} using Eq. (6), and the maximum deflection δ_{max} using Eq. (7).

$$\sigma_{max} = \frac{Mr}{I} = \frac{F_{\perp} x r}{I} \tag{5}$$

$$\tau_{max} \approx \frac{4F_{\perp}}{3\pi r^2} \tag{6}$$

$$\delta_{max} = \frac{F_{\perp} x^2}{6EI}(3L - x) \tag{7}$$

where I is the moment of inertia of the stalk section (m^4); r is the radius of the stalk (m); L is the total length of the stalk (m); E is the elastic modulus of the stalk (MPa).

When these calculated values exceed the allowable stress and deflection limits (Eqs. (8) to (10)), effective separation between the stalk and the branch is achieved.

$$\sigma_{max} \geq [\sigma] \tag{8}$$

$$\tau_{max} \geq [\tau] \tag{9}$$

$$\delta_{max} \geq \delta_{allow} \tag{10}$$

where $[\sigma]$ is the allowable bending stress of the stalk (MPa); $[\tau]$ is the allowable shear stress of the stalk (MPa); δ_{allow} is the allowable deflection of the stalk (m).

In summary, the force analysis demonstrates that the rotational end-effector can apply sufficient load. This load induces significant bending and localized stress concentration at the stalk-branch connection, ultimately leading to separation. This composite force process further highlights the direct influence of parameters such as end-

effector torque and rotational speed on the separation effect. This finding provides a crucial theoretical basis for optimizing the end-effector's parameters

2.4 Simulation of the End-Effector Harvesting Process

To validate the feasibility of the rotational end-effector, this study employs finite element analysis to simulate the harvesting process. The simulation's accuracy largely depends on the chosen parameters [29]. Therefore, it is essential to accurately determine the mechanical properties of the harvesting system. Key parameters were repeatedly measured using a DDL10 electronic universal testing machine following standard operational protocols. All test materials were obtained from the same site to ensure data consistency and reliability. The end-effector was fabricated from polylactic acid (PLA) using 3D printing technology, resulting in a lightweight yet robust component. In combination with previous research and relevant literature [30], the final simulation parameters were established.

The specific steps of the simulation process are outlined as follows:

(1) Modeling. Three-dimensional models of the branch, stalk, apple, and end-effector were constructed using Creo 6.0 software based on the measured data. These models were then assembled. To improve computational efficiency, certain components were simplified while ensuring that key mechanical properties remained unaffected.

(2) Setting Material Properties. The assembled model was imported into Abaqus 2020 software, ensuring that the components did not interfere with one another. Material properties for the branch, stalk, apple, and end-effector were assigned based on measurement results and literature references [29], as detailed in Tab. 2.

Table 2 Specific values of material properties

Component	Density / kg/m^3	Elastic modulus / MPa	Poisson's ratio
Branch	600	1036.0	0.4
Stalk	840	5.0	0.35
Apple	300	46.9	0.40
End-effector	1250	3500.0	0.35

(3) Defining Interactions. A global contact property was created to define both tangential and normal interactions within the contact regions. Specific contact properties were further assigned to the interfaces between the stalk and the branch, and between the stalk and the apple, to accurately reflect frictional and adhesive effects (Fig. 5a).

(4) Applying Loads and Constraints. A predetermined torque was applied along the central axis of the end-effector to simulate the bending force on the stalk. Since the branch typically remains stable during the harvesting process, both ends of the branch were fixed, thereby simplifying the model and reducing simulation time (Fig. 5b).

(5) Meshing. Appropriate mesh types and element sizes were selected for each component to balance simulation accuracy and efficiency. Fine meshes were applied to critical regions to ensure calculation credibility (Fig. 5c).

(6) Initiating the Simulation. After verifying all settings, the simulation was initiated. The stress distribution and deformation were recorded in detail. Subsequent papers will provide an in-depth analysis and discussion of the simulation results.

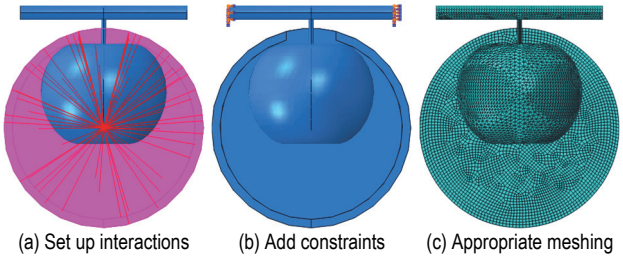

(a) Set up interactions (b) Add constraints (c) Appropriate meshing

Figure 5 Main settings for simulation

2.5 Composition and Operation Process of the Harvesting Robot

In this study, the end-effector is integrated into an independently developed apple harvesting robot (Fig. 6). The overall dimensions of the harvesting robot are 2.0 m (length) × 1.0 m (width) × 1.5 m (height), and the cycle picking time is 6 seconds per apple. The harvesting robot primarily comprises a control system, a mobile chassis, a detection module, a robotic arm, and the end-effector. The control system, built on the Robot Operating System (ROS) platform, is responsible for real-time path planning and coordinated actions. The mobile chassis uses an independent four-wheel drive system that enables precise remote control. The detection module is equipped with a ZED binocular camera and an enhanced deep learning network model for target apple identification [31]. The robotic arm features a lightweight, multi-degree-of-freedom design that facilitates precise control of the end-effector.

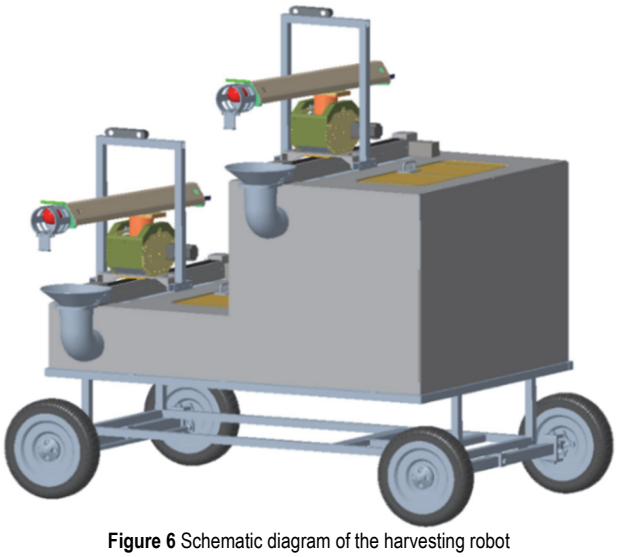

Figure 6 Schematic diagram of the harvesting robot

As illustrated in Fig. 7, the control process of the harvesting robot consists of three main steps:

(1) Detection and Localization. The enhanced network model is used for real-time detection. Stereo vision techniques then accurately determine the three-dimensional position of each apple, providing critical data for subsequent robotic arm localization.

(2) Path Planning and Robotic Arm Motion. Upon receiving the position data, the control system performs motion analysis and path planning. The resulting plan is transmitted over the Controller Area Network (CAN) bus to the robotic arm's servo motors. These motors drive the arm along an optimal path toward the target position and precisely align the end-effector with the harvesting point.

(3) Harvesting Operation. A harvesting command is transmitted via a serial port to the end-effector's motor. The motor rotates the harvesting barrel and applies a predetermined bending force to gently separate the stalk from the branch, thereby ensuring the integrity of the apple.

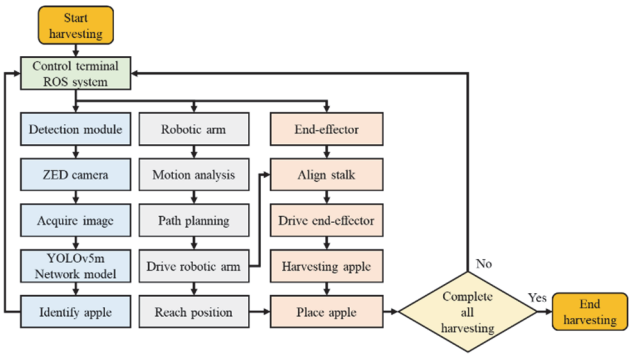

Figure 7 Composition and operation process of the harvesting robot

2.6 Experimental Design for Validation

To validate the practical performance of the end-effector, a series of harvesting experiments were performed in October 2023 and again in October 2024 at Yujia apple orchard (34°34'N, 107°23'E) in Baoji, Shaanxi Province. The experiment site's agronomic conditions were consistent with preliminary measurements. The experiment equipment included a harvesting robot, an end-effector, and auxiliary devices such as a laptop, a camera, and labels. Detailed experiment results and analysis will be discussed in subsequent sections.

Through theoretical analysis, this study identified motor torque, motor speed, and the opening width of the end-effector as the key factors influencing the picking performance. Then, a small-scale field test was conducted to preliminarily determine the effective range of each factor. Specifically, motor torque governs the bending force applied to the stalk. Insufficient torque results in incomplete separation of the stalk from the branch, while excessive torque increases the structural load. Considering both operational efficiency and equipment durability, the optimal motor torque range was determined to be 5-7 N·m. Motor speed affects the harvesting efficiency. Low speeds prolong the separation time and reduce efficiency, whereas excessively high speeds can induce vibrations that compromise stability and accuracy. Experimental data suggest that an operating range of 20-40 rpm is optimal. Furthermore, the opening width of the end-effector is critical for accurate stalk positioning. A narrow opening hinders the stalk from entering the harvesting barrel, while an overly wide opening may allow the stalk to rotate in sync with the end-effector. The ideal opening width was found to be between 20 and 40 mm.

To comprehensively investigate the combined effects of these parameters, a three-factor, three-level experiment was designed using Design-Expert 9.0 software [32]. The harvesting success rate was defined as the evaluation metric (Eq. (11)), and the experimental factors along with their coded levels are detailed in Tab. 3. During the experiments, different motors were employed to adjust the torque, various control commands were used to modify the motor speed, and end-effectors of different sizes were fabricated to adjust the opening width. Multiple experiments were performed for each parameter combination to calculate the average harvesting success rate and record the causes of any failures. The experimental data were then statistically analyzed to assess the effects of each factor and their interactions. Finally, response surface methodology was applied to determine the optimal parameter combination.

$$Y = \frac{n}{N} * 100\% \tag{11}$$

where Y is the harvesting success rate (%); N is the total number of harvesting times; n is the number of successful harvesting times.

Table 3 Three-factor three-level experiment arrangement

Level	*A* - Motor speed / rpm	*B* - Motor torque / N·m	*C* - Opening width / mm
–1	20	5	20
0	30	6	30
1	40	7	40

3 RESULTS AND DISCUSSION

3.1 Simulation Results and Analysis

Finite element simulations indicate that the stalk separation process closely replicates real harvesting conditions.

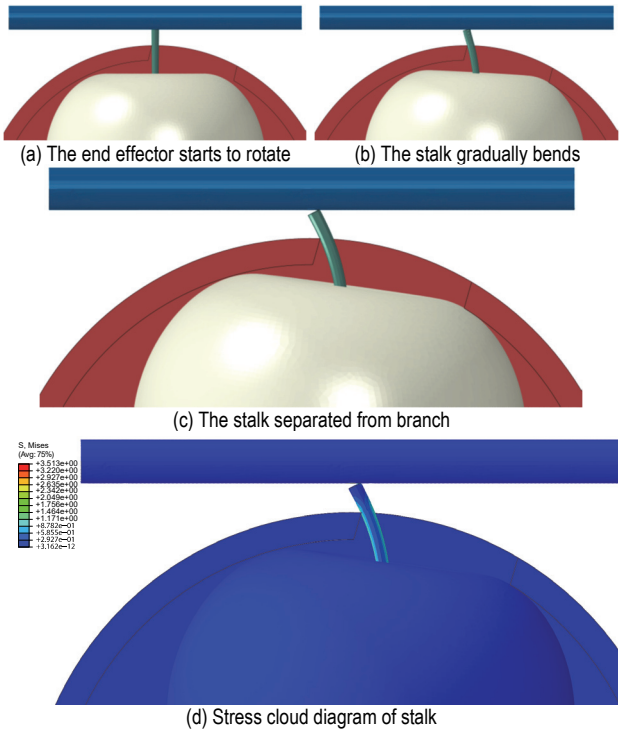

Figure 8 Simulation results of the end-effector harvesting process

As shown in Fig. 8a, once the end-effector accurately positions the stalk, the harvesting barrel rotates, gradually

narrowing the gap between the mechanism and the stalk. Fig. 8b illustrates that upon contact, the harvesting barrel induces a gradual bending deformation in the stalk, which intensifies with an increasing bending angle. Eventually, the composite stress on the stalk exceeds the bonding strength at the branch connection, resulting in successful separation (Fig. 8c). This process validates the feasibility of the rotational end-effector in precisely controlling stalk deformation during harvesting.

Additional analysis of the stress contour plots reveals that the bending force is efficiently transmitted to the critical regions of the stalk. The maximum stress is observed near the branch connection (Fig. 8d), which is the key area for separation. Moreover, the simulation results show that during rotation, the contact duration and area between the end-effector and the apple surface remain minimal. Consequently, the maximum stress on the apple surface stays well below its yield strength, effectively preserving both the external appearance and the internal integrity of the apple.

3.2 Experimental Results and Analysis

Initially, the harvesting robot navigates to the designated work area along a predetermined path. Next, the detection module, equipped with a ZED binocular camera, captures real-time environmental images. An enhanced deep learning model then identifies the harvestable apples. After processing the data, the operating system precisely positions the robotic arm and end-effector at the target location (Fig. 9a). Subsequently, the end-effector rotates following the preset procedure, and the harvesting barrel separates the stalk from the branch (Fig. 9b). Finally, the robotic arm transports the apple to the collection bin (Fig. 9c). This entire harvesting process operates in an efficient and continuous cycle.

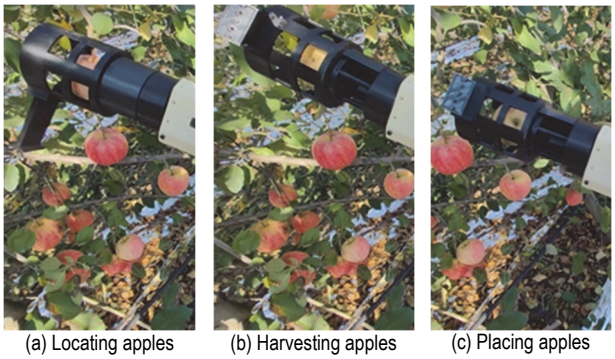

(a) Locating apples (b) Harvesting apples (c) Placing apples

Figure 9 Actual harvesting process of the end effector

Visual inspection reveals that both the stalk and the apple skin remain intact, with no obvious mechanical damage. To further verify the protective effect of the end-effector, the apples were re-examined 72 hours after harvest. The results indicate that the quality of the apples remains stable, with no signs of decay or deterioration. Field experiments demonstrate that the end-effector performs excellently in practical harvesting.

3.3 Parameter Analysis and Performance Optimization

After completing the experiments, the data are compiled in Tab. 4, and the analysis of variance (ANOVA) results are presented in Tab. 5. The model exhibits an *F*-value of 22.68, which is well above the critical threshold of 2. And the *P*-value is less than 0.001, indicating statistical significance at the 0.001 level. In addition, the lack-of-fit P-value exceeds 0.05, suggesting a good model fit. The model demonstrates a correlation coefficient (R^2) of 0.9668, with an adjusted R^2 of 0.9242 and a predicted R^2 of 0.8470 (a difference of less than 0.2). The signal-to-noise ratio is 13.5943, well above the critical value of 4. And the coefficient of variation is only 0.8208%, which is well below 10%. Together, these indicators confirm that the model is highly stable, reliable, and predictive [33].

Table 4 Results of three-factor three-level experiment

Run	*A* - Motor speed / rpm	*B* - Motor torque / N·m	*C* - Opening width / mm	*Y* - Harvesting success rate / %
1	30	6	30	90
2	30	7	40	88
3	20	7	30	84
4	30	6	30	91
5	40	5	30	84
6	30	6	30	90
7	40	6	40	87
8	40	6	20	86
9	30	5	40	87
10	40	7	30	87
11	30	6	30	89
12	30	7	20	87
13	30	5	20	85
14	20	6	40	86
15	20	5	30	82
16	20	6	20	83
17	30	6	30	89

Table 5 ANOVA of experiment results

Source	Sum of squares	Df	Mean square	*F*-value	*P*-value
Model	103.51	9	11.50	22.68	0.0002 (significant)
A - Motor Speed	10.13	1	10.13	19.96	0.0029
B - Motor Torque	8.00	1	8.00	15.77	0.0054
C - Opening Width	6.13	1	6.13	12.08	0.0103
AB	0.2500	1	0.2500	0.4930	0.5053
AC	1.0000	1	1.0000	1.97	0.2030
BC	0.2500	1	0.2500	0.4930	0.5053
A^2	48.67	1	48.67	95.98	< 0.0001
B^2	19.46	1	19.46	38.38	0.0004
C^2	3.41	1	3.41	6.72	0.0358
Residual	3.55	7	0.5071	-	-
Lack of fit	0.7500	3	0.2500	0.3571	0.7880 (not significant)
Pure error	2.80	4	0.7000	-	-
Cor total	107.06	16	-	-	-

Through further analysis, the regression equation of the harvesting success rate was obtained, as shown in Eq. (12).

$$\begin{aligned} Y &= +89.80 + 1.13A + 1.00B + 0.88C \\ &+0.25AB - 0.50AC - 0.25BC \\ &-3.40A^2 - 2.15B^2 - 0.90C^2 \end{aligned} \quad (12)$$

Response surface analysis revealed that the primary factors affecting the harvesting success rate, in order of

importance, are motor speed, motor torque, and end-effector opening width. The detailed findings are as follows:

(1) As shown in Fig. 10, when motor torque is fixed at 6 N·m, the harvesting success rate initially increases with motor speed and then decreases. This behavior is primarily because a moderate increase in motor speed enhances the instantaneous stress, thereby promoting effective separation of the stalk from the branch. However, excessively high speeds compromise the end-effector's stability. The response surface plot indicates that the optimal motor speed range is 30-35 rpm. Further analysis reveals that when motor speed is fixed at 30 rpm, the optimal motor torque range is 6-6.5 N·m.

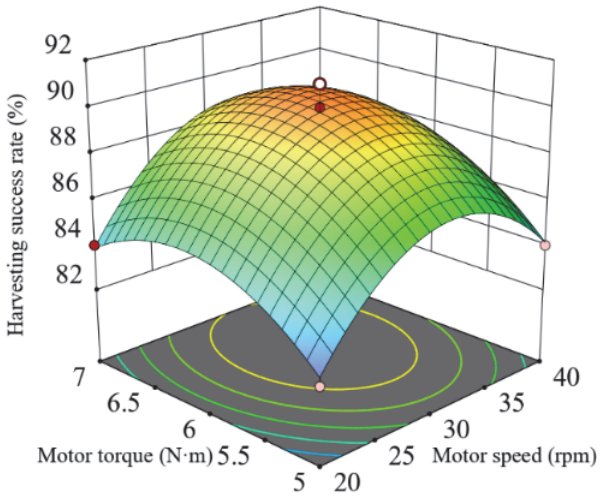

Figure 10 Interaction between motor speed and motor torque

(2) As shown in Fig. 11, when the motor speed is fixed at 30 rpm, the harvesting success rate initially increases and then decreases as the opening width increases. A moderate increase in opening width reduces the difficulty of positioning the end-effector, thereby enhancing success. However, if the opening width is too large, the stalk tends to oscillate under load, adversely affecting operational efficiency. The response surface plot suggests that the optimal opening width range is 32-37 mm. And further analysis reveals that when the opening width is fixed at 30 mm, the optimal motor speed range is 30-33 rpm.

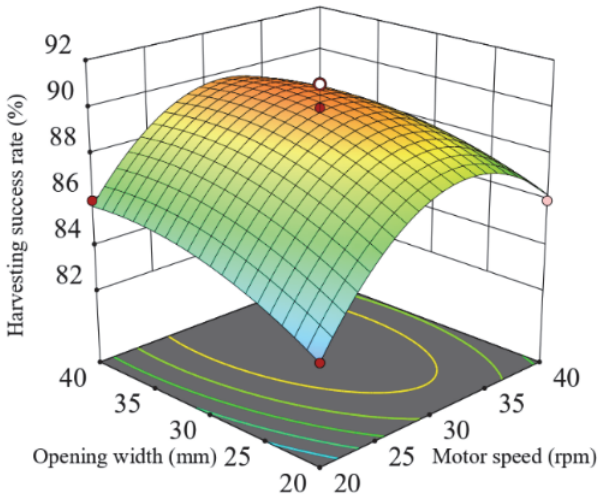

Figure 11 Interaction between motor speed and opening width

(3) As shown in Fig. 12, when the opening width is fixed at 30 mm, the harvesting success rate increases with motor torque up to a point and then decreases. A moderate increase in motor torque enhances the bending action of the end-effector, thereby facilitating stalk separation. However, excessively high torque increases the motor's size and weight, reducing system flexibility. The response surface plot indicates that the optimal motor torque range is 6-6.4 N·m. And further analysis reveals that when motor torque is fixed at 6 N·m, the optimal opening width range is 31-37 mm.

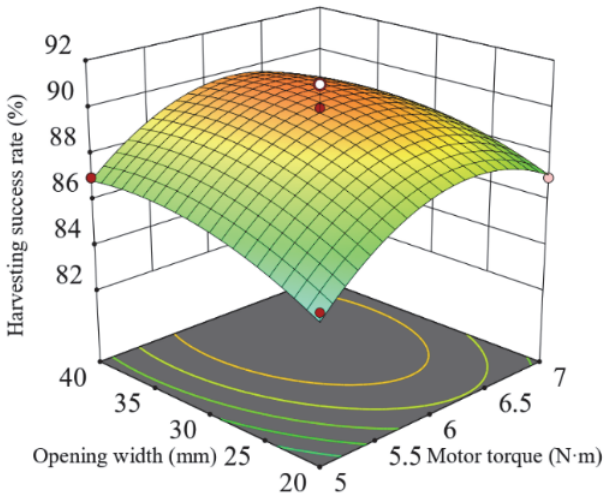

Figure 12 Interaction between motor torque and opening width

Based on these analyses, the optimal parameter combination was found to be a motor speed of 31.43 rpm, a motor torque of 6.22 N·m, and an opening width of 34.16 mm. Under these conditions, the predicted harvesting success rate was 90.17%. Considering the actual operation, field experiments were conducted with a motor speed of 31 rpm, a motor torque of 6 N·m, and an opening width of 34.16 mm. The measured harvesting success rate was 89%, which closely aligns with the model predictions. These results indicate that by appropriately adjusting key parameters, near-ideal harvesting performance can be achieved (Fig. 13).

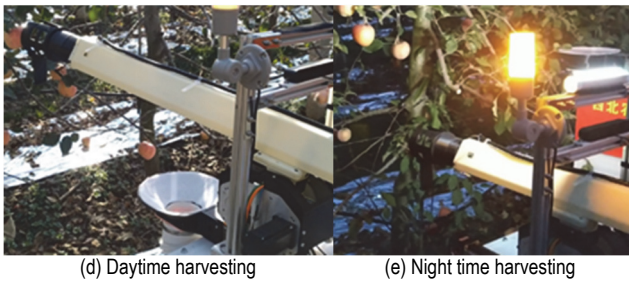

(d) Daytime harvesting (e) Night time harvesting

Figure 13 Verification experiments

Compared with the flexible clamping end-effector reported in Reference (19), the end-effector developed in this study achieves a significantly higher harvesting success rate. Moreover, it avoids the detachment risk associated with the suction-based end-effector described in Reference (15). Such findings provide strong support for the practical application of the end-effector.

3.4 Failure Case Analysis and Improvement Measures

During the harvesting process, failure cases were primarily attributed to three factors:

(1) Positioning Errors. Some harvesting failures occurred due to inaccurate positioning of the end-effector that failed to precisely align with the target apple (Fig. 14a). This issue is mainly caused by occlusions from leaves or branches and lighting variations, which result in missed or false detections by the vision recognition model.

(2) Limited Operational Space. In some instances, the apple growth environment is highly confined. Densely interwoven branches make it difficult for the end-effector to complete a full harvesting action within the restricted space (Fig. 14b).

(3) Insufficient Force Transmission. For some branches that are soft or slender, the end-effector's rotation causes the stalk and branch to rotate together. This reduces the effective bending force, thereby preventing successful separation and harvesting.

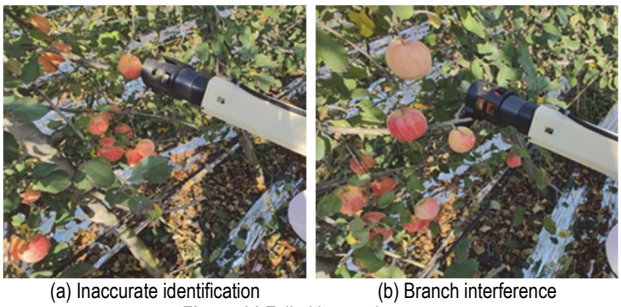

(a) Inaccurate identification (b) Branch interference

Figure 14 Failed harvesting case

To address these issues, the following improvement measures were adopted:

(1) Increase Image Sample Size. Apple images were collected under various lighting conditions, occlusion scenarios, and backgrounds to expand the dataset. This expansion enhances the robustness and adaptability of the vision recognition model, leading to more accurate identification of target apples in complex orchard environments.

(2) Optimize the Harvesting Strategy. The rotation angle and direction of the end-effector are dynamically adjusted based on variations in branch stiffness. This ensures that sufficient bending force is applied without damaging the branches, thereby improving the harvesting success rate.

(3) Improve Structural Design. The structural layout of the end-effector was optimized by adjusting its opening width and geometric shape. These improvements allow for more flexible operation in confined spaces and better adaptation to diverse orchard conditions, ensuring optimal gripping and twisting performance.

(4) Select Flexible Materials. The end-effector was fabricated using lightweight, high-strength flexible materials. This reduces its overall weight and minimizes vibrations during harvesting, thereby significantly enhancing system stability and accuracy.

4 CONCLUSION

This study presents an innovative rotational end-effector for apple harvesting. The end-effector efficiently separates the stalk from the branch by applying a bending force, thereby protecting the quality of apples. Field experiments demonstrate that the harvesting success rate of the end-effector reaches 89%, thereby meeting the design objectives. Although a small number of apples were not successfully picked, the end-effector did not cause any damage and did not compromise the apples' economic value. The main conclusions of this study are as follows:

(1) A comprehensive design scheme and operating principle for the end-effector were established. A force model that incorporates the branch, stalk, apple, and end-effector was developed. Detailed analysis of the critical mechanical conditions required for stalk separation provided a solid theoretical basis for the design.

(2) Finite element analysis was employed to simulate the apple harvesting process. The results show that the bending force applied by the end-effector is sufficient to overcome the bonding force at the stalk-branch interface. Importantly, this process occurs without direct contact with the apple surface, thus preserving the fruit's integrity.

(3) Based on a harvesting robot, multiple field experiments were conducted. The experimental results indicated that when the motor speed was 31.43 rpm, the motor torque was 6.22 N·m, and the opening width was 34.16 mm, the theoretical optimal picking success rate of the end-effector reached 90.17%, while the actual measured success rate was 89%. These results satisfy the design expectations and operational requirements.

The end-effector also demonstrates promising application potential and can be further evaluated for harvesting other fruits, such as oranges. Future research will focus on further enhancing harvesting efficiency, refining vision-based localization, and improving path planning techniques. The ultimate aim is to achieve intelligent and precise agricultural operations.

Acknowledgements

This study is supported by the Qinchuangyuan Project of Shaanxi Province (Grant No. 2023KXJ-016) and the National Natural Science Foundation of China (Grant No. 32272001).

5 REFERENCES

[1] Czernyszewicz, E. (2016). Long-term trends in production and consumption of apples in Poland, *Europe and worldwide Acta Scientiarum Polonorum-Hortorum Cultus*, *15*(3), 95-104.

[2] Zhang, Z., Heinemann, P. H., Liu, J., Baugher, T. A., & Schupp, J. R. (2016). The development of mechanical apple harvesting technology: a review. *Transactions of the ASABE*, *59*(5), 1165-1180. https://doi.org/10.13031/trans.59.11737

[3] Kuta, L., Li, Z. G., Stopa, R., Komarnicki, P., & Slupska, M. (2020). The influence of manual harvesting on the quality of picked apples and the Picker's muscle load. *Computers and Electronics in Agriculture*, *175*, 105511. https://doi.org/10.1016/j.compag.2020.105511

[4] Mo, C. K. (2018). Advances in mechanized tree fruit harvesting. *Hortscience*, *53*(9), 154-155.

[5] Zhou, J. G., Wang, Y. K., Chen, J., Luo, T. Y., Hu, G. R., Jia, J. L., & Sugirbay, A. (2024). Research hotspots and development trends of harvesting robots based on bibliometric analysis and knowledge graphs. *International Journal of Agricultural and Biological Engineering*, *17*(6), 1-10. https://doi.org/10.25165/j.ijabe.20241706.8739

[6] Vrochidou, E., Tsakalidou, V. N., Kalathas, I., Gkrimpizis, T., Pachidis, T., & Kaburlasos, V. G. (2022). An overview of end effectors in agricultural robotic harvesting systems. *Agriculture-Basel*, *12*(8), 1240. https://doi.org/10.3390/agriculture12081240

[7] Navas, E., Fernández, R., Sepúlveda, D., Armada, M., & Gonzalez-de-Santos, P. (2021). Soft grippers for automatic crop harvesting: a review. *Sensors*, *21*(8), 2689. https://doi.org/10.3390/s21082689

[8] Nadeem, M., Quang, T. N., Khaliq, A., Jabbar, A., Iqbal, M., Ghani, M. U., & Ikram, K. (2020). A novel approach to optimize harvesting losses using modified engine operated reaper. *Pakistan Journal of Agricultural Sciences*, *57*(2), 319-326.

[9] Mhamed, M., Zhang, Z., Yu, J., Li, Y., & Zhang, M. (2024). Advances in apple's automated orchard equipment: A comprehensive research. *Computers and Electronics in Agriculture*, *221*, 108926. https://doi.org/10.1016/j.compag.2024.108926

[10] Han, C. Y., Lv, J. H., Dong, C. J., Li, J. H., Luo, Y. Q., Wu, W. B., & Abdeen, M. A. (2024). Classification, advanced technologies, and typical applications of end-effector for fruit and vegetable picking robots. *Agriculture-Basel*, *14*(8), 1310. https://doi.org/10.3390/agriculture14081310

[11] Seol, J., Lee, S., & Son, H. I. (2020). A review of end-effector for fruit and vegetable harvesting robot. *Journal of Korea Robotics Society*, *15*(2), 91-99. https://doi.org/10.7746/jkros.2020.15.2.091

[12] Kultongkham, A., Kumnon, S., Thintawornkul, T., & Chanthasopeephan, T. (2021). The design of a force feedback soft gripper for tomato harvesting. *Journal of Agricultural Engineering*, *52*(1), 7, 1090. https://doi.org/10.4081/jae.2021.1090

[13] Li, M. & Liu, P. (2023). A bionic adaptive end-effector with rope-driven fingers for pear fruit harvesting. *Computers and Electronics in Agriculture*, *211*, 107952. https://doi.org/10.1016/j.compag.2023.107952

[14] Yang, S. Z., Ji, J. C., Cai, H. X., & Chen, H. (2022). Modeling and force analysis of a harvesting robot for button mushrooms. *IEEE Access*, *10*, 78519-78526. https://doi.org/10.1109/Access.2022.3191802

[15] Lu, R. F., Dickinson, N., Lammers, K., Zhang, K. X., Chu, P. Y., & Li, Z. J. (2022). Design and evaluation of end effectors for a vacuum-based robotic apple harvester. *Journal of the Asabe*, *65*(5), 963-974. https://doi.org/10.13031/ja.14970

[16] Graham, S. S., Zong, W., Feng, J., & Tang, S. (2018). Design and testing of a kiwifruit harvester end-effector. *Transactions of the ASABE*, *61*(1), 45-51. https://doi.org/10.13031/trans.12361

[17] Zhao, X., Xu, G. J., Zhang, P. F., Yu, G. H., & Xu, Y. D. (2024). Design and experimental study of the end-effector for broccoli harvesting. *International Journal of Agricultural and Biological Engineering*, *17*(1), 137-144. https://doi.org/10.25165/j.ijabe.20241701.8110

[18] Wang, Y., Yang, Y., Yang, C. H., Zhao, H. M., Chen, G. B., Zhang, Z., Fu, S., Zhang, M., & Xu, H. B. (2019). End-effector with a bite mode for harvesting citrus fruit in random stalk orientation environment. *Computers and Electronics in Agriculture*, *157*, 454-470. https://doi.org/10.1016/j.compag.2019.01.015

[19] Hohimer, C. J., Wang, H., Bhusal, S., Miller, J., Mo, C., & Karkee, M. (2019). Design and field evaluation of a robotic apple harvesting system with a 3d-printed soft-robotic end-effector. *Transactions of the ASABE*, *62*(2), 405-414. https://doi.org/10.13031/trans.12986

[20] Park, Y., Seol, J., Pak, J., Jo, Y., Jun, J., & Son, H. I. (2023). A novel end-effector for a fruit and vegetable harvesting robot: mechanism and field experiment. *Precision Agriculture*, *24*(3), 948-970. https://doi.org/10.1007/s11119-022-09981-5

[21] Gao, J., Zhang, F., Zhang, J. X., Guo, H., & Gao, J. F. (2024). Picking patterns evaluation for cherry tomato robotic harvesting end-effector design. *Biosystems Engineering*, *239*, 1-12. https://doi.org/10.1016/j.biosystemseng.2024.01.009

[22] Li, T., Qiu, Q., Zhao, C. J., & Xie, F. (2021). Task planning of multi-arm harvesting robots for high-density dwarf orchards. *Transactions of the Chinese Society of Agricultural Engineering*, *37*(2), 1-10.

[23] Lin, Y. X., Shang, S. Q., Wang, D. W., Song, L. Q., & Zhang, J. G. (2019). Design of continuous ditching and fixed distance apple planting machine for high density dwarfing orchard. *Transactions of the Chinese Society of Agricultural Engineering*, *35*(1), 23-30.

[24] Beyaz, A. (2018). Harvest glove and LabView based mechanical damage determination on apples. *Scientia Horticulturae*, *228*, 49-55. https://doi.org/10.1016/j.scienta.2017.09.049

[25] Yap, B. W. & Sim, C. H. (2011). Comparisons of various types of normality tests. *Journal of Statistical Computation and Simulation*, *81*(12), 2141-2155. https://doi.org/10.1080/00949655.2010.520163

[26] Bloch, V., Degani, A., & Bechar, A. (2018). A methodology of orchard architecture design for an optimal harvesting robot. *Biosystems Engineering*, *166*, 126-137. https://doi.org/10.1016/j.biosystemseng.2017.11.006

[27] Fan, P., Yan, B., Wang, M. R., Lei, X. Y., Liu, Z. J., & Yang, F. Z. (2021). Three-finger grasp planning and experimental analysis of picking patterns for robotic apple harvesting. *Computers and Electronics in Agriculture*, *188*, 106353. https://doi.org/10.1016/j.compag.2021.106353

[28] Davidson, J., Silwal, A., Karkee, M., Mo, C., & Zhang, Q. (2016). Hand-picking dynamic analysis for under sensed robotic apple harvesting. *Transactions of the ASABE*, *59*(4), 745-758. https://doi.org/10.13031/trans.59.11669

[29] Bu, L. X., Hu, G. R., Chen, C. K., Sugirbay, A., & Chen, J. (2020). Experimental and simulation analysis of optimum picking patterns for robotic apple harvesting. *Scientia Horticulturae*, *261*, 108937. https://doi.org/10.1016/j.scienta.2019.108937

[30] Hu, G., Zhou, J., Chen, Q., Luo, T., Li, P., Chen, Y., Zhang, S., & Chen, J. (2024). Effects of different picking patterns and sequences on the vibration of apples on the same branch. *Biosystems Engineering*, *237*, 26-37. https://doi.org/10.1016/j.biosystemseng.2023.11.010

[31] Hu, G. R., Zhou, J. G., Chen, C., Li, C. L., Sun, L. J., Chen, Y., Zhang, S., & Chen, J. (2022). Fusion of the lightweight network and visual attention mechanism to detect apples in orchard environment. *Transactions of the Chinese Society of Agricultural Engineering*, *38*(19), 131-142.

[32] Xie, H. B., Kong, D. Y., & Wang, Q. (2022). Optimization and experimental study of bionic compliant end-effector for robotic cherry tomato harvesting. *Journal of Bionic Engineering*, *19*(5), 1314-1333. https://doi.org/10.1007/s42235-022-00202-3

[33] Chen, Q. Y., Kang, R., Wei, N. S., Fan, Y. L., Wang, Z. Y., Chen, Y., & Chen, J. (2024). Design and experiment optimize of the vibration harvesting machine of Lyciumbarbarum L. *Journal of Agricultural Engineering*, *55*(4), 1597. https://doi.org/10.4081/jae.2024.1597

Contact information:

Jianguo ZHOU, PhD Candidate
College of Mechanical and Electronic Engineering,
Northwest A&F University Institution,
Yangling 712100, Shaanxi, China
E-mail: jianguozhou@nwafu.edu.cn

Shiwei WEN, MS Candidate
College of Mechanical and Electronic Engineering,
Northwest A&F University Institution,
Yangling 712100, Shaanxi, China
E-mail: wsw142301@nwafu.edu.cn

Deyi ZHANG, MS Candidate
College of Mechanical and Electronic Engineering,
Northwest A&F University Institution,
Yangling 712100, Shaanxi, China
E-mail: zhangdeyi@nwafu.edu.cn

Jun CHEN, PhD, Professor
(Corresponding author)
College of Mechanical and Electronic Engineering,
Northwest A&F University Institution,
Yangling 712100, Shaanxi, China
E-mail: chenjun_jdxy@nwsuaf.edu.cn

Yu CHEN, PhD, Associate Professor
College of Mechanical and Electronic Engineering,
Northwest A&F University Institution,
Yangling 712100, Shaanxi, China
E-mail: jdxy73@nwafu.edu.cn

Guangrui HU, PhD, Lecturer
School of Design,
Xi'an Technological University,
Xi'an 710021, China
E-mail: huguangrui@xatu.edu.cn